Editors' Suggestion

Possible, impossible, and expected diameters and production rates of droplets in aerosols and sprays

Maksim Mezhericher* and Howard A. Stone
Department of Mechanical and Aerospace Engineering, Princeton University, Princeton, New Jersey 08544, USA

(Received 20 December 2021; accepted 13 May 2022; published 15 June 2022)

Liquid atomization processes generating sprays and aerosols of droplets are used in many delivery and coating systems involving pure solvents, solutions, and suspensions. In our recent experimental work, we introduced a novel liquid atomization process generating microsprays and aerosols of submicron-diameter droplets for pure solvents, solutions, and suspensions: gas jets disintegrate thin liquid films that are formed as bubbles approach a liquid surface. Here, we develop a theoretical description of droplet sizes and flow rates, using the first principles of conservation of mass and energy, and employing dimensional and scale analyses. We introduce atomization diagrams as a graphical tool to determine possible, impossible, and expected droplet diameters and specific flow rates in aerosols and sprays produced under various conditions. We find a reasonable agreement between the theory and experiments for five different liquids converted into aerosols of submicron-diameter droplets by an atomization process where gas jets disintegrate thin liquid films that are formed as bubbles approach a liquid surface, and also for five traditional pressure nozzles that produce sprays of droplets of hundreds of microns in diameter. Our study explores the overall range of mean droplet diameters between 0.1 and 100 μm and Ohnesorge numbers between 0.01 and 100, and the analysis and atomization diagrams contribute to understanding of liquid atomization and can serve as a theoretical framework for comparing different liquid atomization techniques.

DOI: 10.1103/PhysRevFluids.7.063602

I. INTRODUCTION

Disintegration of liquids into drops plays a central role in many natural processes as well as in various technological, industrial, and medical applications. Wind and bubble-driven droplet generation over sea surfaces [1,2], splashing of raindrops [3–6], defense mechanisms of some insects [7], spray painting [8], coating of surfaces and particles [9,10], agricultural treatment of plants [11,12], fuel injection during combustion [13,14], atomic spectroscopy [15,16], instant coffee [17,18] and milk powder [19] manufacturing, nasal [20,21] and pulmonary [22,23] drug delivery, blood spatter [24], dental procedures [25], spreading of airborne pathogens while speaking [26–29], singing [26], sneezing [30,31] and coughing [31,32], and other processes involve production of aerosols and sprays by atomization of liquids. The range of applications is clearly varied and enormous.

In many applications the quality, controllability, stability, reproducibility, and scalability of the atomization process is crucial, and scientists and engineers seek to understand the physics of

*maksymm@princeton.edu

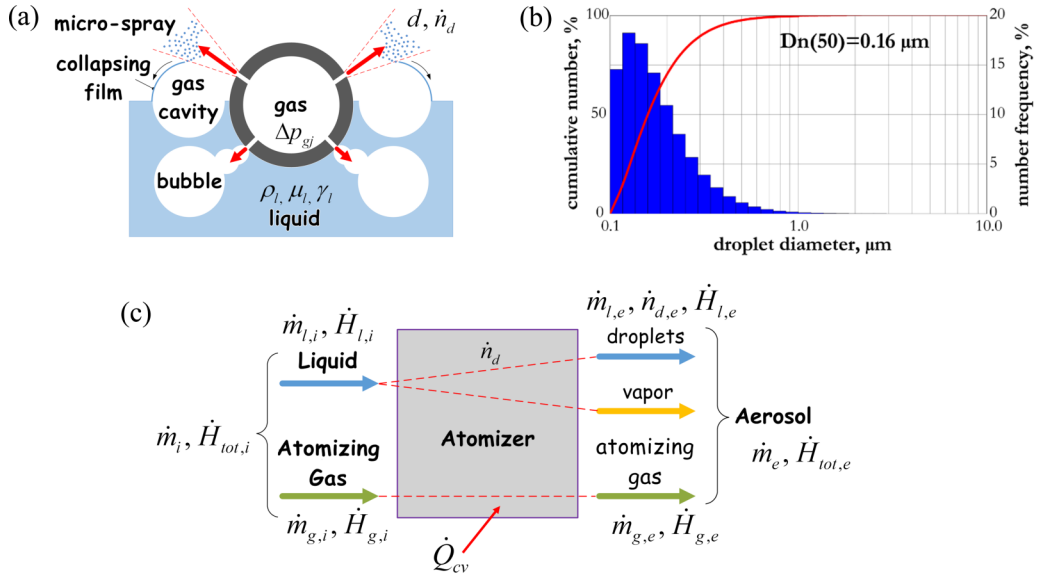

FIG. 1. (a) Liquid atomization process generating submicron droplets when gas jets disintegrate thin liquid films formed as bubbles on a liquid surface [10,33–35]. (b) Typical number-weighted size distribution of water droplets for this liquid atomization process [10,33–35]. (c) Control volume for thermodynamic analysis of the liquid atomization process. In panel (a), compressed gas is supplied into a perforated tube (the tube cross section is shown) partially submerged into a liquid in such a way that the underwater part produces gas bubbles, which rise to the liquid surface. Gas jets, which are produced in the upper part of the perforated tube, disintegrate bubbles over the liquid surface [33,34]. Here, d is the droplet diameter, the pairs $\dot{m}_{l,i}$, $\dot{H}_{l,i}$, $\dot{m}_{g,i}$, $\dot{H}_{g,i}$, and $\dot{m}_i$, $\dot{H}_i$ are, respectively, the mass flow rate and rate of change of enthalpy for liquid, gas, and total flow at the inlet; the pairs $\dot{m}_{l,e}$, $\dot{H}_{l,e}$, $\dot{m}_{g,e}$, $\dot{H}_{g,e}$, and $\dot{m}_e$, $\dot{H}_e$ are, respectively, the analogous quantities at the exit; $\dot{n}_d$, $\dot{n}_{d,e}$ are, respectively, the rate of generated droplets inside and at the exit; $\dot{Q}_{cv}$ is the rate of heat supply; and $\dot{W}_g$ and $\dot{W}_l$ are the rates of work, respectively, done by the gas phase and dissipated by the liquid phase inside the control volume.

liquid disintegration and dispersion, and develop methods and models to improve droplet generating devices. In previous articles [10,33–35] we demonstrated a novel liquid atomization process [Fig. 1(a)]. The process utilizes gas jets to disintegrate bubble-formed thin liquid films, which enables production of polydisperse aerosols of submicron droplets [36] for pure solvents, solutions, and suspensions with wide ranges of viscosity and surface tension [Fig. 1(b)].

For most droplet production processes, an important but unanswered question is how to predict the droplet diameters and flow rates that will be produced for different liquids during atomization. Another question is how to compare between different atomization processes. The available review literature on liquid atomization and spray and aerosol formation processes [37–40] demonstrates the absence of an appropriate theoretical framework to answer these questions because of the complexity of the fluid dynamics involved in the formation of polydisperse sprays and aerosols with time-dependent droplet size distributions [41–47]. Presently, the description of liquid atomization and corresponding devices (atomizers, nozzles, and nebulizers) is mostly empirical and semiempirical [38,48,49], or based on numerical modeling utilizing approaches (e.g., Eulerian–Lagrangian, Reynolds-averaged Navier–Stokes, direct numerical simulations, large-eddy simulations) that are filled with questionable assumptions and require high computational costs that limit their applicability [50–52]. Therefore, there is a need to develop a theoretical description providing determination of possible, impossible, and expected droplet diameters and flow rates produced by a liquid atomization process, and enabling comparison between different liquid atomization techniques.

II. THEORETICAL DEVELOPMENT

A. Thermodynamic analysis of the liquid atomization process

The atomization process is analyzed by applying the law of mass conservation and the first law of thermodynamics for a control volume including the liquid and gas phases, as shown in Fig. 1(c). The rate of change of mass, m_{cv}, in the control volume is determined by the difference of mass flow rates at the inlet, $\dot{m}_i$, and exit, $\dot{m}_e$:

$$\frac{dm_{cv}}{dt} = \dot{m}_i - \dot{m}_e. \tag{1}$$

The rate of change of the number of droplets, $n_{d,cv}$, in the control volume is given by the difference of the net rate of droplets entering at the inlet, $\dot{n}_{d,i}$, and exit, $\dot{n}_{d,e}$, plus the number rate of droplets produced in the control volume, $\dot{n}_d$:

$$\frac{dn_{d,cv}}{dt} = \dot{n}_{d,i} - \dot{n}_{d,e} + \dot{n}_d. \tag{2}$$

The rate of change of energy of the control volume, E_{cv}, is determined by the balance of the rate of (heat) energy supplied to the control volume, $\dot{Q}_{cv}$, the rate of work done by the control volume, $\dot{W}_{cv}$, and the difference of rates of enthalpy addition between the inlet, $\dot{H}_i$, and exit, $\dot{H}_e$ [53]:

$$\frac{dE_{cv}}{dt} = \dot{Q}_{cv} - \dot{W}_{cv} + \dot{H}_i - \dot{H}_e. \tag{3}$$

The rate of work on the control volume is a sum of the rates of work done by the liquid, $\dot{W}_l$, and gas, $\dot{W}_g$, phases:

$$\dot{W}_{cv} = \dot{W}_l + \dot{W}_g. \tag{4}$$

Assuming steady-state flow for a continuous adiabatic process at fixed temperature, neglecting the changes in potential energy of both fluids, evaporation and the change in liquid kinetic energy, assuming complete ideal expansion of the gas jet, disregarding drag and frictional energy dissipation, then from Eqs. (1)–(3) we obtain $\dot{m}_i = \dot{m}_e$ and $\dot{W}_{cv} = 0$. Therefore, inside the control volume the rate of work supplied by the gas phase equals the rate of work done by the liquid phase, $\dot{W}_g = -\dot{W}_l$. In turn, the latter is determined by the sum of the rates of work done by capillary, $\dot{W}_c$, and viscous, $\dot{W}_v$, forces of the liquid, $\dot{W}_l = -(\dot{W}_c + \dot{W}_v)$. Thus, we obtain that $\dot{W}_g = \dot{W}_c + \dot{W}_v$, and dividing by the liquid (droplet) mass flow rate, $\dot{m}_l$, we get

$$w_{\Delta p} = w_c + w_v, \tag{5}$$

where $w_{\Delta p}$ is the specific work (per unit mass) done by the gas phase on the liquid phase because of the supplied differential pressure Δp_{gj} to produce gas jets [Fig. 1(a)], and w_c and w_v are, respectively, the specific works done by capillary and viscous forces in the atomized liquid.

B. Master equation for droplet diameters

In previous research [33], we established two governing dimensionless groups: Ohnesorge number, $\mathrm{Oh}_d = \mu_l/\sqrt{\rho_l \gamma_l \ell}$, and $N_d = \Delta p_{gj} \ell/\gamma_l$, where ρ_l, γ_l, and μ_l are, respectively, liquid density, surface tension, and dynamic viscosity, and ℓ is a characteristic length. These two dimensionless numbers are central to determination of droplet diameters produced in the liquid atomization process shown in Fig. 1(a). Using the timescales of the liquid atomization, including the timescale of energy supplied by the gas jets $\tau_{\Delta p} \sim (\rho_l \ell^2/\Delta p_{gj})^{1/2}$, the Rayleigh capillary breakup

time $\tau_c \sim (\rho_l \ell^3/\gamma_l)^{1/2}$ and the timescale of viscous dissipation $\tau_v \sim \rho_l \ell^2/\mu_l$ in the liquid, the dimensionless groups can be expressed as timescale ratios, $\mathrm{Oh}_d^{-2} \sim \frac{\tau_v^2}{\tau_c^2}$ and $N_d \sim \frac{\tau_c^2}{\tau_{\Delta p}^2}$. Alternatively, the energy scales and timescales are connected, i.e., the scales of the energy associated with the gas pressure $e_{\Delta p} = \ell^2/\tau_{\Delta p}^2$, the energy stored or released by surface effects $e_c = \ell^2/\tau_c^2$, and the energy dissipated by liquid viscosity $e_v = \ell^2/\tau_v^2$, so that $\mathrm{Oh}_d^{-2} \sim \frac{e_c}{e_v}$ and $N_d \sim \frac{e_{\Delta p}}{e_c}$. Assuming that energy scales are proportional to the respective specific works, then $e_c \sim w_c$, $e_v \sim w_v$, and $e_{\Delta p} \sim w_{\Delta p}$. Correspondingly, we conclude that the physical meaning of the dimensionless numbers are ratios of specific work, and $\mathrm{Oh}_d^{-2} = k_1 \frac{w_c}{w_v}$ and $N_d = k_2 \frac{w_{\Delta p}}{w_c}$, where k_1 and k_2 are coefficients of proportionality. Substituting these expressions into Eq. (5), we establish a relationship between the dimensionless numbers:

$$N_d = k_2 + k_1 k_2 \mathrm{Oh}_d^2 \,. \tag{6}$$

Equation (6) relates the specific works performed by the gas jets and dissipated by the atomized liquid, and is the master equation which enables constructing a diagram for determination of droplet diameters on the plane (Oh_d^{-2}, N_d). Though the proportionality coefficients are unknown, there are either empirical or theoretical ways to determine their values. Our theoretical study, reported elsewhere [54], which involves the development and solution of a stochastic differential equation for the droplet size distribution function, suggests that in general $O(k_1) = O(k_2) = 1$, and provides a theoretical framework to determine the constant k_2. Here, we do not apply that complicated stochastic method, yet we investigate different values of proportionality coefficients for the range $k_2 = 0.1{-}10$ while keeping $k_1 = 1$, and compare the predicted droplet diameters with a wide range of experimental data.

C. Master equation for droplet flow rates

To determine droplet flow rates for the liquid atomization process shown in Fig. 1(a), we take time derivatives of all the terms of Eq. (5), and obtain the balance of the rates of change of specific energy:

$$\dot{w}_{\Delta p} = \dot{w}_c + \dot{w}_v. \tag{7}$$

Here, $\dot{w}_{\Delta p}$ is the rate of specific work done by the atomizing gas on the liquid by means of the supplied differential gas pressure Δp_{gj}, and $\dot{w}_c$ and $\dot{w}_v$ are, respectively, the rates of specific work done by capillary and viscous forces in the atomized liquid. Employing the dimensionless analysis described in our previous paper [33], we establish two dimensionless numbers $N_{l,cv} = \rho_l^{5/2} \gamma_l^{3/2} d^{9/2} \xi/\mu_l^3$ and $N_l = \Delta p_{gj}^{3/2}/(\rho_l \gamma_l^{3/2} d^{3/2} \xi)$, which determine the specific flow rate of droplets, $\xi = \dot{n}_{d,e}/\dot{m}_{d,e}$, for the expected droplet diameters $N_d^{**} = \Delta p_{gj} \langle d \rangle/\gamma_l = 1$, and $\dot{n}_{d,e}$ and $\dot{m}_{d,e}$ are, respectively, the number and the mass-flow rates of droplets at the outlet of the atomizer [see Fig. 1(b)]. Performing the algebra with steps similar to those undertaken above for the droplet diameters, we conclude that in terms of the ratio of timescales of the involved phenomena, $N_{l,cv} \sim \frac{\tau_v^3}{\tau_c^3}$ and $N_l \sim \frac{\tau_c^3}{\tau_{\Delta p}^3}$. On the other hand, the scale of energy rate supplied by gas pressure is given by $\varepsilon_{\Delta p} = \ell^2/\tau_{\Delta p}^3$, the scale of energy rate stored or released by surface tension is $\varepsilon_c = \ell^2/\tau_c^3$, and the scale of energy rate dissipated by liquid viscosity $\varepsilon_v = \ell^2/\tau_v^3$. We assume that ratios of energy rate scales are proportional to the corresponding ratios of rates of specific works, i.e., $N_{l,cv} \sim \frac{\varepsilon_c}{\varepsilon_v} = k_5 \frac{\dot{w}_c}{\dot{w}_v}$, and $N_l \sim \frac{\varepsilon_{\Delta p}}{\varepsilon_c} = k_6 \frac{\dot{w}_{\Delta p}}{\dot{w}_c}$, where k_5 and k_6 are coefficients of proportionality. Substituting these expressions into Eq. (7), we find

$$N_l = k_6 + k_5 k_6 N_{l,cv}^{-1}. \tag{8}$$

The established Eq. (8) relates the rates of specific work provided by the gas jets and dissipated by the atomized liquid in nondimensional form, and it determines the specific flow rates of the produced

droplets. Again, as a first approximation, we assume that the proportionality coefficients are order of 1, $O(k_5) = O(k_6) = 1$, and we investigate different values of proportionality coefficients for the range $k_6 = 0.1-10$ while keeping $k_5 k_6 = 1$, and compare the predicted droplet diameters with a wide range of experimental data.

III. RESULTS AND DISCUSSION

A. Atomization diagrams for droplet diameters

1. Aerosols

We assume that the characteristic length is equal to a droplet diameter, $\ell = d$, and construct an atomization diagram for water, when the droplet diameter, d, and gas jet differential pressure, Δp_{gj}, are varied; see Fig. 2(a). The central line is given by the relationship $N_d^* = 1 + \mathrm{Oh}_d^2$, which is obtained from Eq. (6) by setting $k_1 = k_2 = 1$ as a first approximation. This line provides the expectation of droplet diameters at different atomizing gas pressures Δp_{gj}. In a simple case, the expected diameter for a polydisperse aerosol or spray, $\langle d \rangle$, is the "count" mean droplet diameter, $\bar{d}_{1,0}$, of the respective number-weighted droplet size distribution, i.e., $\langle d \rangle = \bar{d}_{1,0}$ [37,39]. For water and common aqueous solutions, $\mathrm{Oh}_d^2 \ll 1$, so the central line in the atomization diagram is given by the limit $N_d^{**} = 1$. Recalling that $N_d \sim \frac{e_{\Delta p}}{e_c}$, we outline the atomization region of possible droplet diameters by considering $e_{\Delta p} \approx e_c$, i.e., $O(N_d) = 1$, and determine two boundaries of the atomization region: the lower boundary, below which the supplied energy is insufficient to perform atomization, $e_{\Delta p} \ll e_c$; and the upper boundary, above which there is an excess of atomization energy, $e_{\Delta p} \gg e_c$, meaning that a liquid particle will be disintegrated into smaller fragments. These two conditions can be satisfied by considering an order of magnitude difference from the central line, so we take $N_d = 0.1 N_d^{**}$ and $N_d = 10 N_d^*$ as, respectively, the lower and the upper boundaries of the atomization region [Fig. 2(a)]. It is worth noting that those two boundaries encompass a wide range of the coefficients of proportionality, i.e., $N_d = 0.1 N_d^{**}$ is equivalent to setting $k_2 = 0.1$, and $N_d = 10 N_d^*$ is equivalent to setting $k_2 = 10$ in Eq. (6).

Using the data on the count mean diameter, $\bar{d}_{1,0}$, for water droplets measured using a Malvern Spraytec device [34], we plot the experimental points on the atomization diagram given in Fig. 2(a). It can be observed that those points either fall on or lie very close to the expectancy line, $N_d^{**} = 1$, and hence there is a good agreement between the theoretically expected and measured count mean droplet diameters using $O(1)$ proportionality constants.

In addition to water, we extend our study by constructing atomization diagrams for droplet diameters of other liquids, including gasoline, diesel, and aqueous solutions of sodium alginate and sodium benzoate, and explore the overall range of Ohnesorge number between 0.01 and 100 ($\mathrm{Oh}_d^{-2} = 10^{-4} - 10^4$; see the Appendix). By plotting experimental points based on the droplet diameters measured in our previous studies [10,33], we find that all those points are located within the atomization region in the vicinity of the line of theoretical expectation [given by Eq. (6) with $k_1 = k_2 = 1$].

2. Sprays

The theoretical procedure for constructing atomization diagrams for droplet diameters can also be applied to other liquid atomization processes, for example pressure nozzles as given in Fig. 2(b). The diagram was constructed on the plane (Oh_d^{-2}, We_d), where $\mathrm{We}_d = \rho_g u_{\mathrm{rel}}^2 d/\gamma_l = 2\rho_g \Delta p_l d/(\rho_l \gamma_l)$ is the Weber number for an ideal nozzle discharge into a still ambient gas based on the droplet diameter, d, and relative velocity $u_{\mathrm{rel}} = \sqrt{2\Delta p_l/\rho_l}$ between the liquid jet exiting the nozzle and the ambient gas, and Δp_l is nozzle pressure. Using the steps we took to develop Eq. (6), we obtain for pressure nozzles

$$\mathrm{We}_d = k_4 + k_3 k_4 \mathrm{Oh}_d^2 . \tag{9}$$

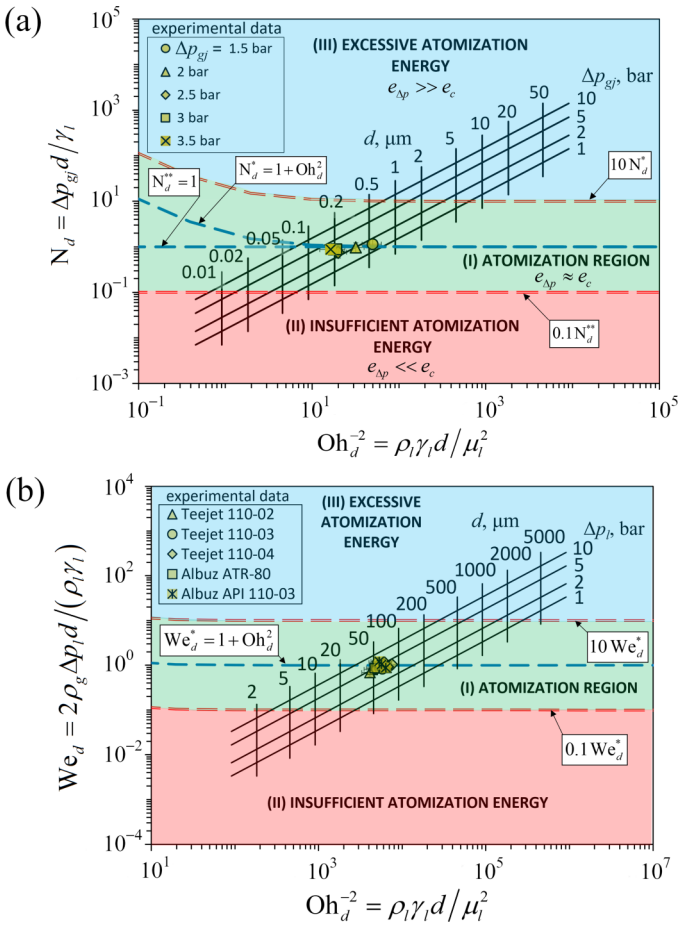

FIG. 2. Atomization diagrams for the diameters of water droplets generated in two different liquid atomization processes. (a) Aerosols of water droplets generated by our own process [Fig. 1(a)]; the experimental data (symbols) were obtained for different atomizing gas pressures in our previous study [34]. (b) Sprays of water droplets produced by conventional pressure nozzles; labels correspond to experimental data (symbols) for various nozzle models reported in Ref. [44]. Error bars denote measurement uncertainties as we evaluated here (experimental errors were not provided in Ref. [44]). Region (I) encompasses the area of the expected droplet diameters, and droplets in the regions (II) and (III) have either too small or too large diameters with respect to the atomization energy that is required to overcome the work of capillary and viscous forces in the liquid.

As above, to construct the atomization diagram in Fig. 2(b), we consider that the proportionality coefficients are order of 1, $O(k_3) = O(k_4) = 1$, and obtain the expectancy line $We_d^* = 1 + Oh_d^2$ by setting $k_3 = k_4 = 1$ as a first approximation. Overall, we investigate different values of proportionality coefficients by setting $k_4 = 0.1,\ 1,\ 10$ while keeping $k_3 = 1$ and comparing the predictions with experimental data. The lower boundary of the atomization region, below which there is insufficient atomization energy to overcome the energy associated with capillary forces, $e_{\Delta p} \ll e_c$, and the upper boundary of the atomization region above which there is an excess of atomization energy, $e_{\Delta p} \gg e_c$, are determined by assuming tenfold ratios of the expected Weber number, respectively $0.1We_d^*$ and $10We_d^*$. It is worth noting that those two boundaries encompass a wide scope of the coefficients of proportionality, i.e., $0.1We_d^*$ is equivalent to setting $k_4 = 0.1$, and $10We_d^*$ is equivalent to setting $k_4 = 10$ in Eq. (9). Also, for water and common aqueous solutions with $Oh_d^2 \ll 1$, the

expectacy line expression from Eq. (9) is reduced to $\mathrm{We}_d^{**} = 1$, and thus the upper boundary of the atomization region is given by the line $10\mathrm{We}_d^{**} = 10$. Such a value of the upper boundary is justified by the well-known theoretical [55,56] and experimental observations [37,38,57] in liquid atomization that droplets with $\mathrm{Oh}_d \ll 1$ and $\mathrm{We}_d > 10$ are unstable and undergo so-called "secondary atomization" caused by aerodynamic drag breakup mechanisms [49,58]. On the other hand, droplets with $\mathrm{Oh}_d^2 \ll 1$ and Weber number below the lower boundary line of atomization region, $0.1\mathrm{We}_d^{**} = 0.1$, may undergo only small oscillatory shape deformation without breakup [49].

Comparing Eqs. (6) and (9), we conclude that the Weber number for sprays plays a similar role to the dimensionless group N_d established before for aerosol production. Using the measured mass median droplet diameters of water sprays, $\bar{d}_{50}$, reported in a study [44] for different pressure nozzles, employing the Hatch-Choate [39,59] relationship $\bar{d}_{1,0} = \bar{d}_{50}\exp[-2.5(\ln\sigma_g)^2]$ for a lognormal droplet size distribution, and taking the geometric standard deviation $\sigma_g = 1.7$ (based on Fig. 17 in Ref. [44]), we plot the experimental data in Fig. 2(b). All the experimental points have $\mathrm{Oh}_d^2 \ll 1$ and either fall on or lie very close to the expectancy line, $\mathrm{We}_d^{**} = 1$. Again, we conclude that there is good agreement between the theoretically expected and measured count mean droplet diameters with $O(1)$ proportionality constants.

B. Atomization diagrams for droplet flow rates

1. Aerosols

Figure 3(a) illustrates the atomization diagram for flow rates of water droplets, which was constructed using Eq. (8) and by setting $k_6 = \pi/6$ and $k_5k_6 = 1$. The former value was obtained by noticing the fact that in the limit $N_{l,cv} \gg 1$, which holds for many common liquids like water and aqueous solutions, we find from Eq. (4) that $N_l^{**} = \Delta p_{gj}^{3/2}/(\rho_l\gamma_l^{3/2}\langle d\rangle^{3/2}\langle\xi\rangle) = k_6$. By using $\langle\xi\rangle = \bar{\xi}_{1,0} = 1/(\frac{\pi}{6}\rho_l\bar{d}_{1,0}^3)$, which is the natural connection between the expected specific flow rate, $\langle\xi\rangle$, and the expected droplet diameter, $\langle d\rangle$, given by $N_d^{**} = \Delta p_{gj}\langle d\rangle/\gamma_l = 1$, we obtain the equation for the expected specific droplet flow rate, $N_l^{**} = \pi/6 = k_6$. Recalling that $N_l \sim \frac{\varepsilon_{\Delta p}}{\varepsilon_c}$, we outline the atomization region of possible specific droplet flow rates by considering the expectation $\varepsilon_{\Delta p} \approx \varepsilon_c$, i.e., $O(N_l) = 1$, and determine the boundaries by $N_l = 0.1N_l^{**}$ (the lower boundary of insufficient atomization energy rate with $\varepsilon_{\Delta p} \ll \varepsilon_c$) and $N_l = 10N_l^{**}$ (the upper boundary of excess of atomization energy with $\varepsilon_{\Delta p} \gg \varepsilon_c$). Using the experimental data [34], we construct Fig. 3(a) and observe good agreement between the theoretically expected and measured specific droplet flow rates; the experimental points either fall on or lie very close to the expectancy line, $N_l^{**} = \pi/6$.

In a similar way to atomization diagrams for droplet diameters, we broaden our study by constructing atomization diagrams for droplet flow rates of gasoline, diesel, and aqueous solutions of sodium alginate and sodium benzoate with an overall range of Ohnesorge number 0.01–100 (see the Appendix). By plotting the experimental points based on the measurements in our previous studies [10,33], we find that all those points are located within the atomization region in the vicinity of the line of theoretical expectation [given by Eq. (8) for $k_6 = \pi/6$ and $k_5k_6 = 1$].

2. Sprays

The procedure for constructing an atomization diagram for droplet flow rates was also applied to pressure nozzles and the results for water spray droplets are shown in Fig. 3(b). The diagram was developed for the plane $(N_{l,cv},\ N_l)$, with the dimensionless numbers $N_{l,cv} = \rho_l^{5/2}\gamma_l^{3/2}d^{9/2}\xi/\mu_l^3$ and $N_l = (2\rho_g\Delta p_l)^{3/2}/(\rho_l^{5/2}\gamma_l^{3/2}d^{3/2}\xi)$ established by employing the dimensional analysis for a pressure nozzle. Also, Fig. 3(b) demonstrates the experimental data based on the diameters and flow rates of water droplets for different models of pressure nozzles reported in Ref. [44]. All the experimental points are located in the atomization region corresponding to the expected droplet flow rates, and are concentrated either on or near the expectancy line, $N_l^{**} = \pi/6$.

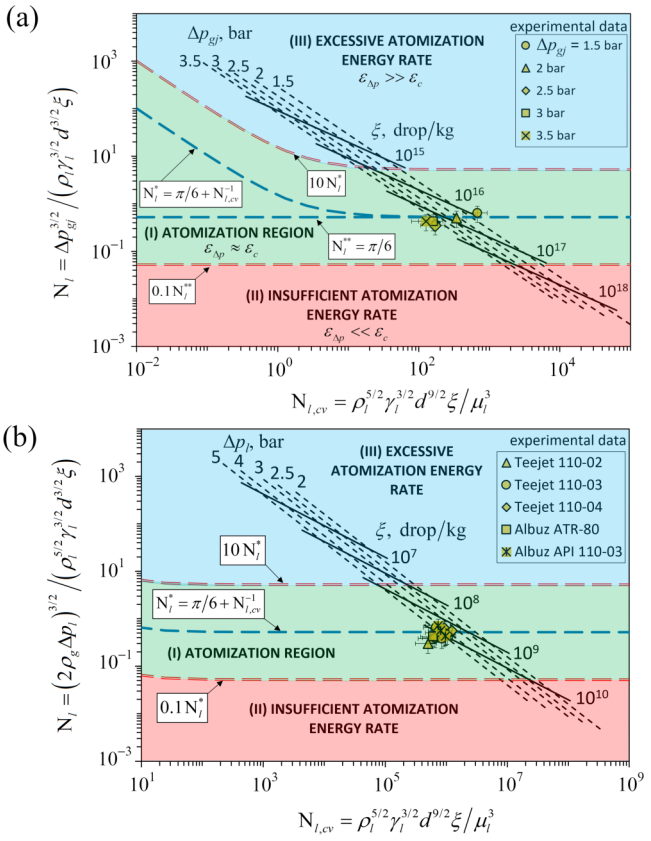

FIG. 3. Atomization diagrams for specific flow rates of water droplets generated in two different liquid atomization processes. (a) Aerosols of water droplets generated by our atomization process [Fig. 1(a)]; the experimental data (symbols) were obtained for different atomizing gas pressures [34]. (b) Sprays of water droplets produced by pressure nozzles; labels correspond to experimental points (symbols) reported for various nozzle models in Ref. [44]. The experimental points are based on the measured count mean droplet diameters, $\bar{d}_{1,0}$, and error bars denote the evaluated measurement uncertainties. Region (I) encompasses the area of the expected specific droplet flow rates, and droplets in the regions (II) and (III) have either too large or too small specific droplet flow rates with respect to the invested atomization energy rate required to overcome the work rates of capillary and viscous forces in the liquid.

C. Comparison between theoretical and experimental droplet diameters and flow rates

The results in Fig. 4(a) summarize the atomization diagram for droplet diameters of all the studied liquids, and the expected and the measured mean droplet diameters for various liquids are compared in Figs. 4(b) and 4(c) for both our liquid atomization process and for spraying by pressure nozzles reported in the literature [44]. In addition, the summary diagram and the comparison between the expected and the measured specific flow rates for different liquids and liquid atomization methods are shown in Fig. 5.

In general, the results in Figs. 4 and 5 show an agreement between the theoretically expected and measured mean droplet diameters and specific flow rates for both droplet aerosols and sprays. Figures 4(a) and 5(a) demonstrate that all the experimental points fall inside the atomization region, which is the range of the expected droplet diameters and specific flow rates, and, respectively, in between the boundaries $d_{\min}$ and $d_{\max}$ in Figs. 4(b) and 4(c) and, with some exclusion explained later, in between $\xi_{\min}$ and $\xi_{\max}$ in Figs. 5(b) and 5(c). Furthermore, most of the experimental points,

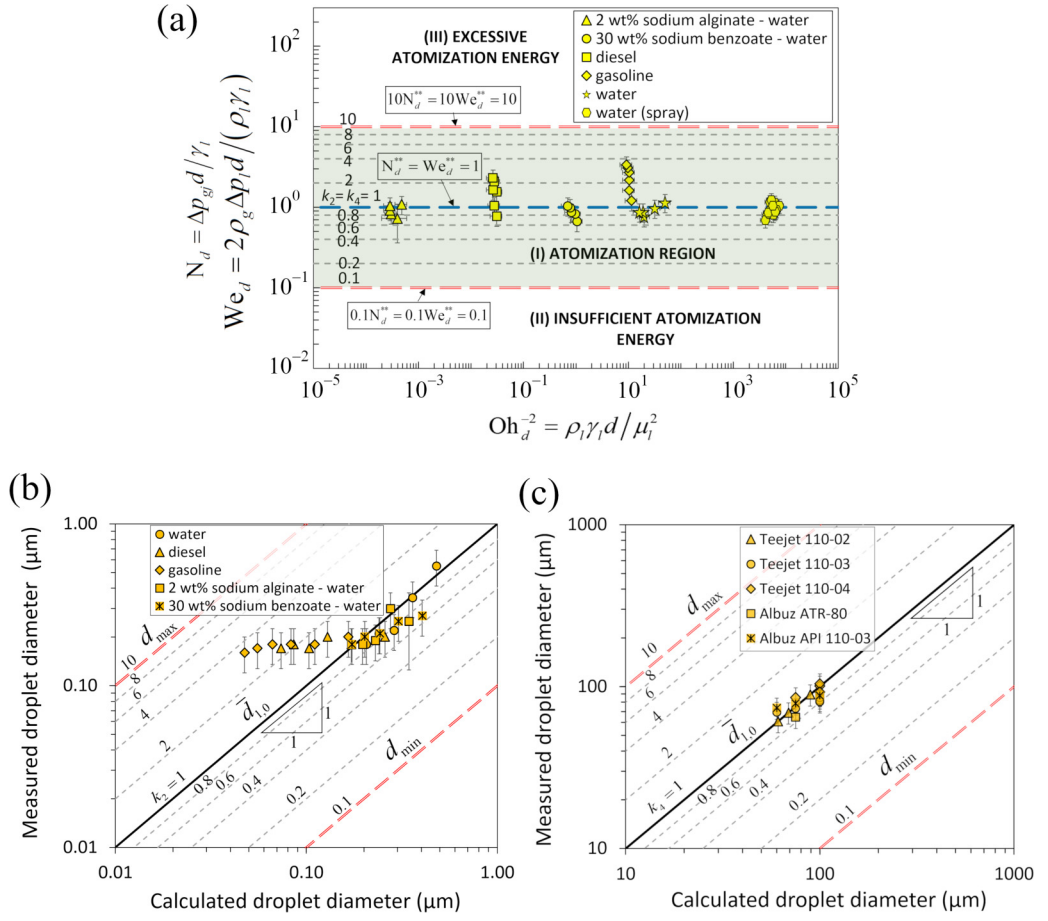

FIG. 4. (a) Atomization diagram summarizing droplet diameters for various liquids produced by the two studied atomization processes. The combined vertical axis has two labels, N_d for aerosol generation shown in Fig. 1(a) [33,34] and We_d for spraying from pressure nozzles [44]. (b) Comparison between theoretical predictions and experimental data [10,33,34] for count mean droplet diameters, $\bar{d}_{1,0}$, of various liquids subjected to the atomization process shown in Fig. 1(a). (c) Comparison between theoretical predictions and experimental data for pressure nozzles [44] for count mean droplet diameters, $\bar{d}_{1,0}$. The lines $\bar{d}_{1,0}$ correspond to the lines of the expected dimensionless numbers N_d^{**} and We_d^{**} [obtained by setting proportionality coefficients $k_1 = k_2 = k_3 = k_4 = 1$ in Eqs. (6) and (9)]. The double-dashed lines denote theoretical lower and upper boundaries of possible droplet diameters, d_{min} and d_{max}, for the produced polydisperse aerosols and sprays, and correspond to the boundary lines of the atomization regions [obtained by setting each of k_2 and k_4 to 0.1 and 10 while keeping $k_1 = k_3 = 1$ in Eqs. (6) and (9)]. Error bars indicate the evaluated measurement uncertainties.

within the measurement uncertainties, are concentrated either on or near the respective expectancy lines [respectively, the central lines $N_d^{**} = We_d^{**} = 1$ and $N_l^{**} = \pi/6$ in Figs. 4(a) and 5(a), and the lines of $\bar{d}_{1,0}$ and $\bar{\xi}_{1,0}$ in Figs. 4(b), 4(c), 5(b), and 5(c)]. However, when the calculated mean droplet diameters are smaller than 0.1 μm, the results in Fig. 4(b) [and, respectively, in Figs. 4(a), 5(a), and 5(b)] show deviations of some experimental points from the theoretically expected values for droplets of gasoline and diesel. Because these fuels had the smallest values of surface tension among all the studied liquids (17 and 26 mN/m; see Table I in the Appendix), their atomization produced aerosols with the smallest droplet diameters [33]. The measurement device (Malvern Spraytec)

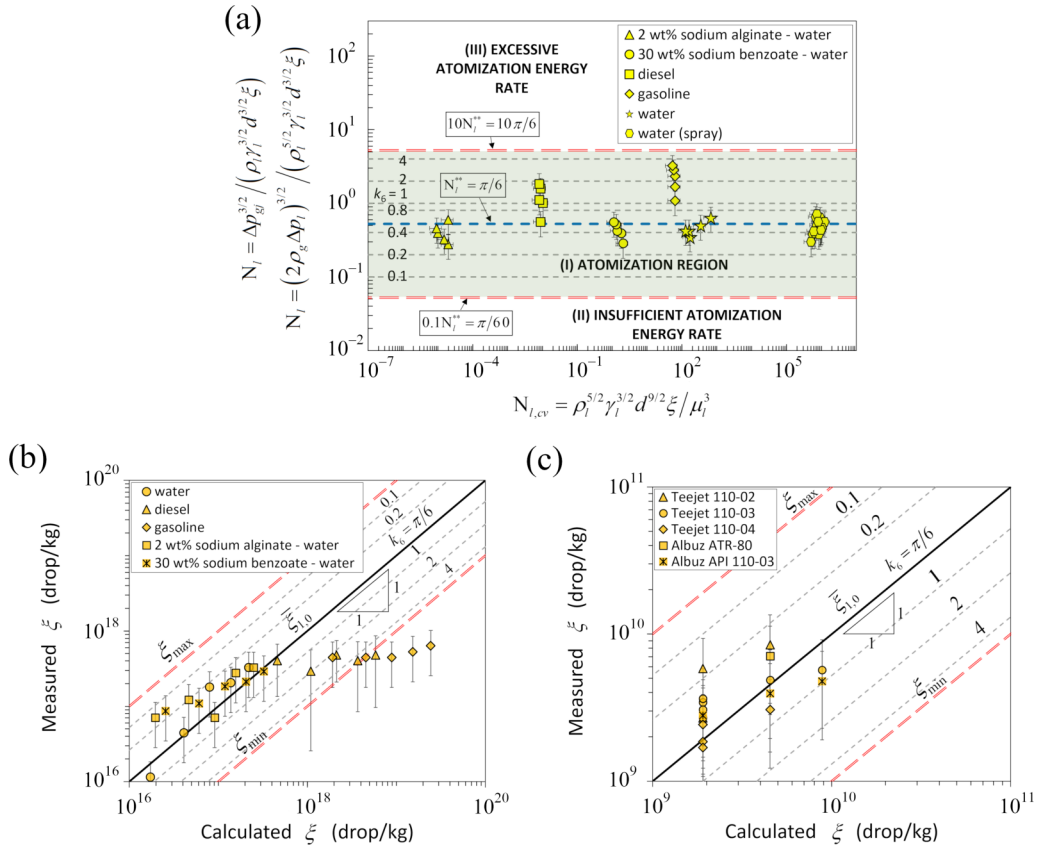

FIG. 5. (a) Atomization diagram summarizing specific droplet flow rates for various liquids produced by the two studied atomization processes. The combined vertical axis has two labels of dimensionless numbers respectively for aerosol generation shown in Fig. 1(a) [33,34] and for spraying from pressure nozzles [44]. (b) Comparison between theoretical predictions and experimental data [10,33,34] for expected specific flow rate $\bar{\xi}_{1,0} = 1/(\frac{\pi}{6}\rho_l \bar{d}_{1,0}^3)$ of various liquids subjected to the atomization process shown in Fig. 1(a). (c) Comparison between theoretical predictions and experimental data for pressure nozzles [44] for $\bar{\xi}_{1,0}$. The lines $\bar{\xi}_{1,0}$ correspond to the lines of the expected dimensionless numbers N_l^{**} in the atomization diagrams [obtained by setting proportionality coefficients $k_6 = \pi/6$ and $k_5 k_6 = 1$ in Eq. (8)]. The double-dashed lines denote the theoretical lower and upper boundaries of possible specific flow rates, $\xi_{\min}$ and $\xi_{\max}$, for the produced polydisperse aerosols and sprays, and correspond to the boundary lines of the atomization regions [obtained by setting k_6 to $\pi/60$ and $10\pi/6$ while keeping $k_5 k_6 = 1$ in Eq. (8)]. Error bars indicate the evaluated measurement uncertainties.

was unable to resolve droplets with diameters smaller than 0.1 μm [33,60] due to the optical limit of the utilized Mie scattering laser technique [61,62]. As a result, the measured droplet size distributions did not adequately represent the fractions of small droplets by disregarding droplets with diameters <0.1 μm in fine polydisperse aerosols or sprays. Hence, there is a systematic bias in the experimental mean droplet diameters, which shifted the diameter data towards higher values, and this bias grows with an increase of the fraction of sub-0.1-μm droplets in the droplet size distributions, as observed from Figs. 4(b) and 5(b). Therefore, the experimental data encompassing Ohnesorge numbers 0.01–100 suggest that the proportionality coefficients $k_1, \ldots, k_6$ are close to unity, and thus setting $k_1 = k_2 = k_3 = k_4 = 1$ for droplet diameters and $k_6 = \pi/6$ while keeping $k_5 k_6 = 1$ for specific droplet flow rates is a reasonable choice at a first approximation to find the expected, possible, and impossible droplet diameters of a steady adiabatic liquid atomization process

with negligible droplet evaporation, without the need to solve detailed differential equations of the process.

The developed theoretical approach assumes that energy supplied to an atomization process is completely spent overcoming surface tension and viscous forces, which is needed to disintegrate bulk liquid into droplets. For many atomization processes under normal conditions additional dissipation effects can be negligible [37,44,45], but for some atomization processes or under certain (usually extreme) conditions these other dissipation mechanisms can impact the droplet diameters and flow rates [45]. In this sense, our theoretical model describes an idealized liquid atomization process, and predicts possible, impossible, and expected droplet diameters and specific flow rates accounting only for surface tension and viscous effects, without considering additional irreversible energy dissipation phenomena.

D. Comparison between different liquid atomization techniques

The theoretical framework and atomization diagrams can serve as a tool for comparison between liquid atomization techniques. As an example, we compare droplets of water produced at the same differential pressure applied in the two considered atomization systems, our aerosol generation technique [Fig. 1(a)] and conventional pressure nozzle producing sprays [44]. Setting the differential nozzle pressure equal to the atomizing gas pressure drop, $\Delta p_l = \Delta p_{gj}$, and equating the governing dimensionless numbers in both systems, $N_d = \mathrm{We}_d$, while the Ohnesorge number is the same, thus we find based on Eqs. (6) and (9) that the expected droplet diameters for a conventional pressure nozzle are ~400 times bigger than those for our liquid atomization device [cf. Figs. 4(b) and 4(c)]. Also, the expected number of droplets generated from 1 kg of water by pressure nozzles is several orders of magnitude smaller than for our liquid atomization process producing aerosols of submicron-diameter droplets, because $\xi \sim 1/d^3$ [cf. Figs. 5(b) and 5(c)].

IV. CONCLUSIONS

In this study we developed a theoretical framework to determine possible, impossible, and expected droplet diameters and specific flow rates in liquid atomization processes for aerosols and sprays based on the first principles of conservation of mass and energy, and dimensionless and scale analyses. Our theory was confirmed by experimental data obtained in our previous studies [10,33,34] and the literature [44] for mean droplet diameters between 0.1 and 100 μm and Ohnesorge numbers in the range 0.01–100.

ACKNOWLEDGMENTS

The research reported in this publication was supported by the Foundation for Health Advancement and New Jersey Health Foundation via the Allergan Foundation Innovation Grant Program, Grant No. ALL 01–21, and the National Center for Advancing Translational Sciences (NCATS), a component of the National Institutes of Health (NIH) under Award No. UL1TR003017. The content is solely the responsibility of the authors and does not represent the official views of the National Institutes of Health.

APPENDIX

Please see Figs. 6–9 and Table I for properties of liquids and additional atomization diagrams.

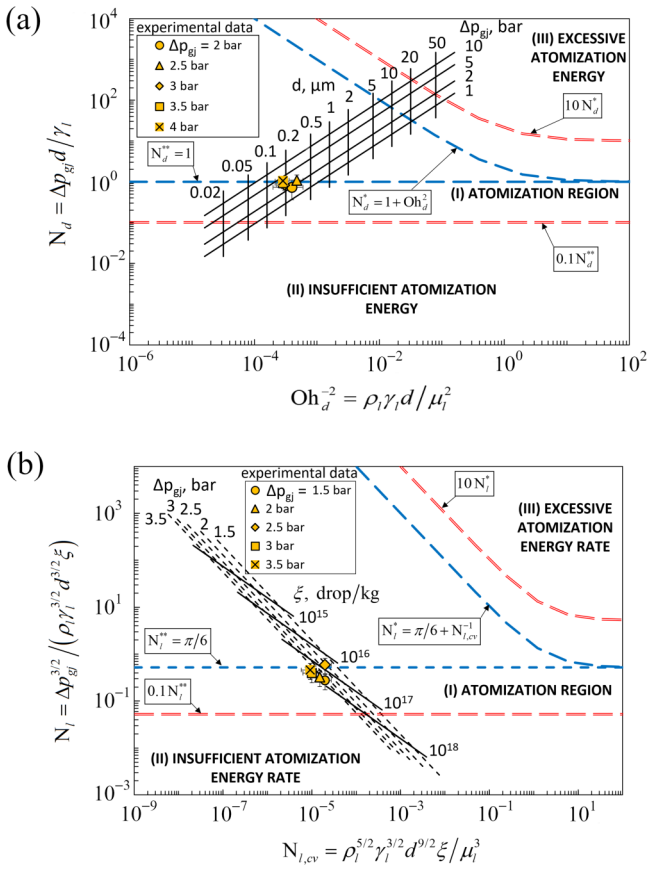

FIG. 6. Atomization diagrams for droplets of aqueous solution of sodium alginate (2 wt.%) generated by the atomization process shown in Fig. 1(a): (a) droplet diameters, d, and (b) specific droplet flow rates, ξ.

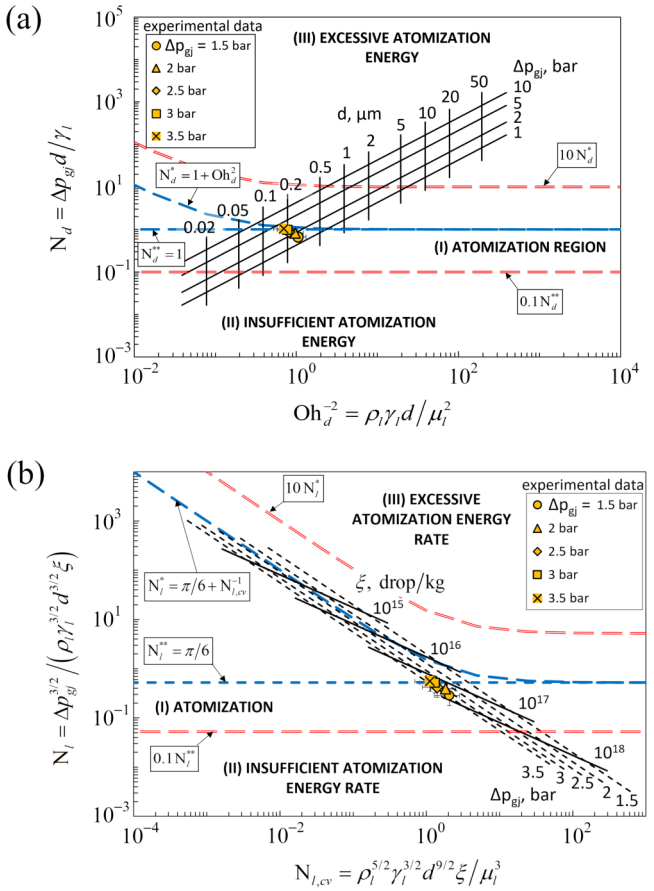

FIG. 7. Atomization diagrams for droplets of aqueous solution of sodium benzoate (30 wt.%) generated by the atomization process shown in Fig. 1(a): (a) droplet diameters, d, and (b) specific droplet flow rates, ξ.

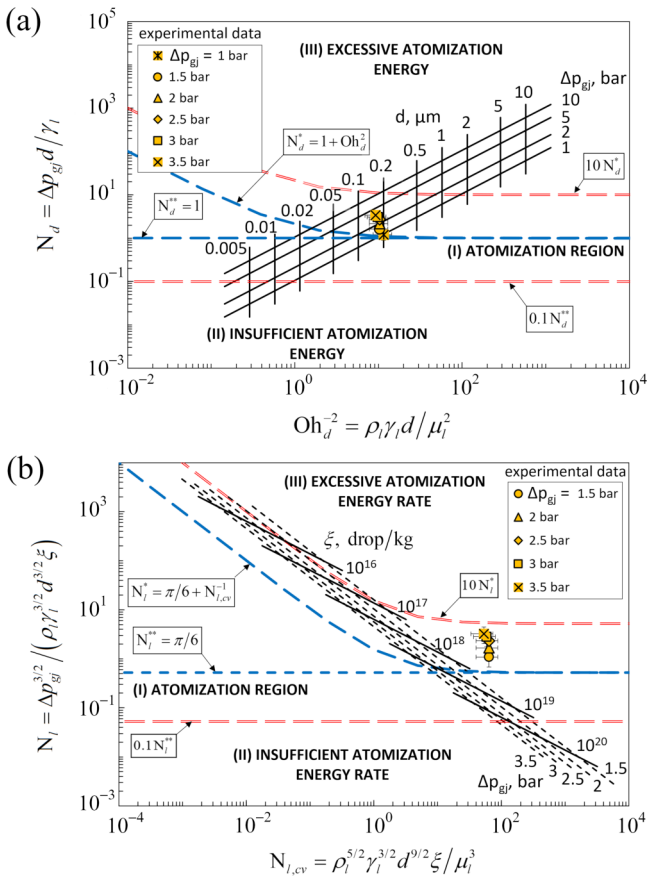

FIG. 8. Atomization diagrams for gasoline droplets generated by the atomization process shown in Fig. 1(a): (a) droplet diameters, d, and (b) specific droplet flow rates, ξ.

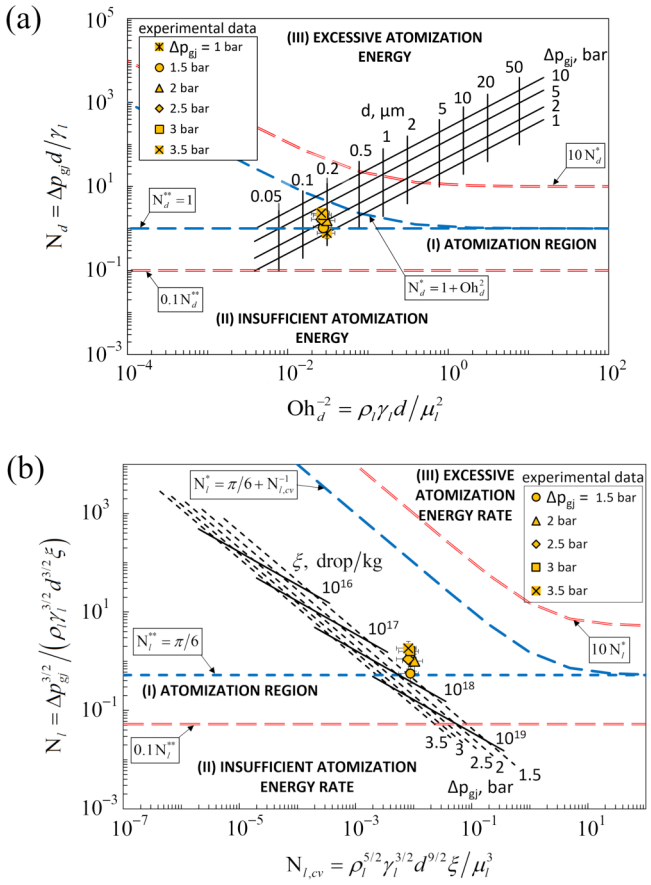

FIG. 9. Atomization diagrams for diesel droplets generated by the atomization process shown in Fig. 1(a): (a) droplet diameters, d, and (b) specific droplet flow rates, ξ.

TABLE I. Properties of liquids used in experiments (adapted from Refs. [10,33,34]).

Liquid	Density, kg/m^3	Surface tension[a], mN/m	Viscosity, mPa s
Diesel	814 ± 19	25.8 ± 1.1	11.66 ± 0.06
Gasoline (95 RON)	734 ± 19	16.6 ± 0.9	0.46 ± 0.01
2 wt.% sodium alginate in water	1004 ± 15	68.9 ± 2.4	208.60 ± 1.04
30 wt.% sodium benzoate in water	1125 ± 17	60.7 ± 1.8	4.19 ± 0.09
Water	998	72.86	1.00

[a]The values of surface tension were obtained in air at room temperature.

[1] J. Wu, Evidence of sea spray produced by bursting bubbles, Science **212**, 324 (1981).
[2] F. Veron, Ocean spray, Annu. Rev. Fluid Mech. **47**, 507 (2015).
[3] M. Marzen and T. Iserloh, Processes of raindrop splash and effects on soil erosion, in *Precipitation*, edited by J. Rodrigo-Comino (Elsevier, 2021), Chap. 15, pp. 351–371.
[4] S.-C. Zhao, R. de Jong, and D. van der Meer, Liquid-Grain Mixing Suppresses Droplet Spreading and Splashing During Impact, Phys. Rev. Lett. **118**, 054502 (2017).
[5] T. Gilet and L. Bourouiba, Fluid fragmentation shapes rain-induced foliar disease transmission, J. R. Soc. Interface **12**, 20141092 (2015).
[6] A. L. Yarin, Drop impact dynamics: Splashing, spreading, receding, bouncing …, Annu. Rev. Fluid Mech. **38**, 159 (2006).
[7] N. Beheshti and A. C. Mcintosh, The bombardier beetle and its use of a pressure relief valve system to deliver a periodic pulsed spray, Bioinspir. Biomim. **2**, 57 (2007).
[8] R. L. Hines, Electrostatic atomization and spray painting, J. Appl. Phys. **37**, 2730 (1966).
[9] F. Aziz and A. F. Ismail, Spray coating methods for polymer solar cells Fabrication: A review, Mater. Sci. Semicond. Process. **39**, 416 (2015).
[10] M. Mezhericher, C. Rieck, N. Razorenov, and E. Tsotsas, Ultrathin coating of particles in fluidized bed using submicron droplet aerosol, Particuology **53**, 23 (2020).
[11] K. Massel, I. Godwin, and L. Hickey, Tunable crops are just a spray away, Nat. Plants **7**, 102 (2021).
[12] C. Beans, Agricultural spray could quickly deliver advantageous genes to crops mid-growing season, Proc. Natl. Acad. Sci. USA **118** (2021).
[13] A. G. MacPhee *et al.*, X-ray imaging of shock waves generated by high-pressure fuel sprays, Science **295**, 1261 (2002).
[14] M. M. Elkotb, Fuel atomization for spray modelling, Prog. Energy Combust. Sci. **8**, 61 (1982).
[15] R. Woodriff, Atomization chambers for atomic absorption spectrochemical analysis: A review, Appl. Spectrosc. **28**, 413 (1974).
[16] J. B. Willis, Atomization problems in atomic absorption Spectroscopy—I. A study of the operation of a typical nebulizer, spray chamber and burner system, Spectrochim. Acta Part A: Mol. Spectrosc. **23**, 811 (1967).
[17] S. Padma Ishwarya and C. Anandharamakrishnan, Spray-freeze-drying approach for soluble coffee processing and its effect on quality characteristics, J. Food Eng. **149**, 171 (2015).
[18] C. S. MacLeod, J. A. McKittrick, J. P. Hindmarsh, M. L. Johns, and D. I. Wilson, Fundamentals of spray freezing of instant coffee, J. Food Eng. **74**, 451 (2006).
[19] V. Birchal, M. L. Passos, G. Wildhagen, and A. Mujumdar, Effect of spray-dryer operating variables on the whole milk powder quality, Drying Technol. **23**, 611 (2005).
[20] K. Inthavong, M. C. Fung, X. Tong, W. Yang, and J. Tu, High resolution visualization and analysis of nasal spray drug delivery, Pharm. Res. **31**, 1930 (2014).
[21] P. G. Djupesland, Nasal drug delivery devices: Characteristics and performance in a clinical perspective—a review, Drug Deliv. Transl. Res. **3**, 42 (2013).
[22] S. P. Hertel, G. Winter, and W. Friess, Protein stability in pulmonary drug delivery via nebulization, Adv. Drug. Delivery Rev. **93**, 79 (2015).
[23] A. R. Martin and W. H. Finlay, Nebulizers for drug delivery to the lungs, Expert Opinion Drug Delivery **12**, 889 (2015).
[24] P. M. Comiskey, A. L. Yarin, and D. Attinger, Theoretical and experimental investigation of forward spatter of blood from a gunshot, Phys. Rev. Fluids **3**, 063901 (2018).
[25] J. Plog, J. Wu, Y. J. Dias, F. Mashayek, L. F. Cooper, and A. L. Yarin, Reopening dentistry after COVID-19: Complete suppression of aerosolization in dental procedures by viscoelastic medusa gorgo, Phys. Fluids **32**, 083111 (2020).
[26] M. Alsved, A. Matamis, R. Bohlin, M. Richter, P.-E. Bengtsson, C.-J. Fraenkel, P. Medstrand, and J. Löndahl, Exhaled respiratory particles during singing and talking, Aerosol Sci. Technol. **54**, 1245 (2020).
[27] M. Abkarian, S. Mendez, N. Xue, F. Yang, and H. A. Stone, Speech can produce jet-like transport relevant to asymptomatic spreading of virus, Proc. Natl. Acad. Sci. USA **117**, 25237 (2020).

[28] F. Yang, A. A. Pahlavan, S. Mendez, M. Abkarian, and H. A. Stone, Towards improved social distancing guidelines: Space and time dependence of virus transmission from speech-driven aerosol transport between two individuals, Phys. Rev. Fluids **5**, 122501(R) (2020).
[29] M. Abkarian and H. A. Stone, Stretching and break-up of saliva filaments during speech: A route for pathogen aerosolization and its potential mitigation, Phys. Rev. Fluids **5**, 102301(R) (2020).
[30] B. E. Scharfman, A. H. Techet, J. W. M. Bush, and L. Bourouiba, Visualization of sneeze ejecta: Steps of fluid fragmentation leading to respiratory droplets, Exp. Fluids **57**, 24 (2016).
[31] L. Bourouiba, The fluid dynamics of disease transmission, Annu. Rev. Fluid Mech. **53**, 473 (2021).
[32] L. Bourouiba, E. Dehandschoewercker, and J. W. M. Bush, Violent expiratory events: On coughing and sneezing, J. Fluid Mech. **745**, 537 (2014).
[33] M. Mezhericher, N. Razorenov, G. Mazor, Y. Ju, and H. A. Stone, Submicron aerosols of liquid fuels: Method of production, experimental characterization and a semi-empirical model, Appl. Energy **235**, 1651 (2019).
[34] M. Mezhericher, I. Ladizhensky, and I. Etlin, Atomization of liquids by disintegrating thin liquid films using gas jets, Int. J. Multiphase Flow **88**, 99 (2017).
[35] M. Mezhericher, J. K. Nunes, J. J. Guzowski, and H. A. Stone, Aerosol-assisted synthesis of submicron particles at room temperature using ultra-fine liquid atomization, Chem. Eng. J. **346**, 606 (2018).
[36] X. Jiang, L. Rotily, E. Villermaux, and X. Wang, Submicron drops from flapping bursting bubbles, Proc. Natl. Acad. Sci. USA. **119**, e2112924119 (2022).
[37] A. H. Lefebvre and V. G. McDonell, *Atomization and Sprays*, 2nd ed. (CRC Press, Boca Raton, 2017).
[38] *Handbook of Atomization and Sprays: Theory and Applications*, edited by N. Ashgriz (Springer, New York, 2011).
[39] W. C. Hinds, *Aerosol Technology: Properties, Behavior, and Measurement of Airborne Particles* (Wiley, 2012).
[40] W. H. Finlay, *The Mechanics of Inhaled Pharmaceutical Aerosols: An Introduction* (Elsevier Science, 2019).
[41] G. I. Taylor, The dynamics of thin sheets of fluid. III. Disintegration of fluid sheets, Proc. R. Soc. London, Ser. A **253**, 313 (1959).
[42] A. M. Gañán-Calvo, Generation of Steady Liquid Microthreads and Micron-Sized Monodisperse Sprays in Gas Streams, Phys. Rev. Lett. **80**, 285 (1998).
[43] E. Villermaux, Ph. Marmottant, and J. Duplat, Ligament-Mediated Spray Formation, Phys. Rev. Lett. **92**, 074501 (2004).
[44] S. Kooij, R. Sijs, M. M. Denn, E. Villermaux, and D. Bonn, What Determines the Drop Size in Sprays? Phys. Rev. X **8**, 031019 (2018).
[45] E. Villermaux, Fragmentation versus cohesion, J. Fluid Mech. **898**, P1 (2020).
[46] H. Lhuissier and E. Villermaux, Bursting bubble aerosols, J. Fluid Mech. **696**, 5 (2012).
[47] J. Eggers and E. Villermaux, Physics of liquid jets, Rep. Prog. Phys. **71**, 036601 (2008).
[48] C. Dumouchel, On the experimental investigation on primary atomization of liquid streams, Exp. Fluids **45**, 371 (2008).
[49] D. R. Guildenbecher, C. López-Rivera, and P. E. Sojka, Secondary atomization, Exp. Fluids **46**, 371 (2009).
[50] X. Jiang, G. A. Siamas, K. Jagus, and T. G. Karayiannis, Physical modelling and advanced simulations of gas–liquid two-phase jet flows in atomization and sprays, Prog. Energy Combust. Sci. **36**, 131 (2010).
[51] K. Luo, C. Shao, M. Chai, and J. Fan, Level set method for atomization and evaporation simulations, Prog. Energy Combust. Sci. **73**, 65 (2019).
[52] M. Gorokhovski and M. Herrmann, Modeling primary atomization, Annu. Rev. Fluid Mech. **40**, 343 (2008).
[53] C. Borgnakke and R. E. Sonntag, *Fundamentals of Thermodynamics*, 10th ed. (John Wiley & Sons Inc., 2020).
[54] M. Mezhericher and H. A. Stone, Size distribution of raindrops, arXiv:2204.03151.
[55] I. Sher and E. Sher, Analytical criterion for droplet breakup, Atomiz Sprays **21**, 1059 (2011).

[56] F. Marcotte and S. Zaleski, Density contrast matters for drop fragmentation thresholds at low Ohnesorge number, Phys. Rev. Fluids **4**, 103604 (2019).
[57] S. A. Krzeczkowski, Measurement of liquid droplet disintegration mechanisms, Int. J. Multiphase Flow **6**, 227 (1980).
[58] M. Jain, R. S. Prakash, G. Tomar, and R. V. Ravikrishna, Secondary breakup of a drop at moderate Weber numbers, Proc. R. Soc. A **471**, 20140930 (2015).
[59] T. Hatch and S. P. Choate, Statistical description of the size properties of non uniform particulate substances, J. Franklin Inst. **207**, 369 (1929).
[60] Spraytec User Manual, MANO368. Issue 3.0, Malvern Instruments Ltd.; (2007) (n.d.).
[61] G. B. J. de Boer, C. de Weerd, D. Thoenes, and H. W. J. Goossens, Laser diffraction spectrometry: Fraunhofer diffraction versus Mie scattering, Part. Part. Syst. Charact. **4**, 14 (1987).
[62] C. F. Bohren and D. R. Huffman, *Absorption and Scattering of Light by Small Particles* (Wiley, 2008).